DOI: 10.13009/EUCASS2017-314

Experimental and theoretical investigations of solid-phase ice accretion

Alexey Kashevarov, Vladimir Levchenko, Alexey Miller, Yuri Potapov and Albert Stasenko
Central Aerohydrodynamic Institute (TsAGI)
1, Zhukovsky str., Zhukovsky, Moscow region, Russia,140181

Abstract

Experimental investigations on run-back ice formation were conducted for the wing airfoil model with heated leading edge in fully glaciated icing conditions in the cases of initially dry warm surface and surface covered by the artificially created liquid film. The work was aimed at obtaining data on ice mass rate at the different surface and flow parameters to validate numerical models of ice crystals accretion in flight conditions. The water film thickness, velocity and temperature on the surface of the model in the cross air/crystal flow were calculated on the basis of the elaborated theoretical model.

1. Introduction

This article is devoted to the TsAGI experimental and theoretical results obtained in frames of the 7 FP High Altitude Ice Crystals Project and Russian Science Foundation Project 16-19-10472. The experimental investigation of ice accretion on the wing profile model with a heated wall was performed in fully glaciated conditions for different flow velocity, ice water content (IWC) and temperature values. The problem of impinged crystals interaction with warmed surface, initially dry or covered by the flowing liquid film, is very important for understanding of icing physical processes occurring in engines and Pitot tubes during the flight in crystal and mixing clouds. In the present work the crystals impingement on the surface was realized in the case of the external flow around an airfoil. In this way easy observations and measurements as well as good understanding of icing physics were provided.
Theoretical investigations concern the modelling of liquid film on a heated wall in the presence of ice crystals. On the basis of the developed physico-mathematical model we carried out calculations of the evolution of the film thickness, velocity and temperature along the front part of the experimental model for the set of parameters typical to the performed experiments. The obtained results are significant for improvement of experimental and computational techniques and physical models creation of icing under crystal impingement.

2. Experimental investigations

2.1 Experimental set-up

Two plants were used for the experiments. One is season-dependent test bench EU-1 and another is year-round artificial icing rig. The facility EU-1 (Fig. 1) consists of the aerodynamic channel with multiple-nozzle ejector, water spraying system with swirl injectors, system of the supplying and regulation of the ejecting air pressure. The wind tunnel is the ejector, which has 25 nozzles. The ejecting gas is compressed air at the pressures from 1.5 to 5 ga. atm. The ejected air at the temperatures from –5 to –25^{o} C is captured from outdoor in the cold season. The ejection coefficient is 7. The total length of wind tunnel channel equals 2910 mm. The cross-section sizes are 200×200 mm. The flow velocity in the channel is controlled in the range from 10 to 100 m/s due to changing the ejecting air pressure. The type of facility is climatic wind tunnel, so the investigations can be carried out only at the negative temperatures of the ambient air. Crystals were injected through L-shaped tube (for the case of the artificial crystals produced by ice block shaving) or supplied with the use of conveyor.
The year-round artificial icing rig is a chamber, where the fan-driven open loop wind tunnel, the crystal supply system and water spraying system, producing the drops of prescribed sizes are settled, figure 2. The desired air temperature up to –18^{o} C in the chamber is reached due to pumping of cold air from a refrigerating machine. The wind tunnel jet flow is cleaved with grids and a fairing to enhance mixing with ambient air. The rig allows conducting weather independent investigations of the icing processes in laboratory conditions. Chamber volume of 360 m^3 ensures operation of wind tunnel with discharge area of 0.09 m^2 at flow velocities up to 80 m/s.

DOI: 10.13009/EUCASS2017-314

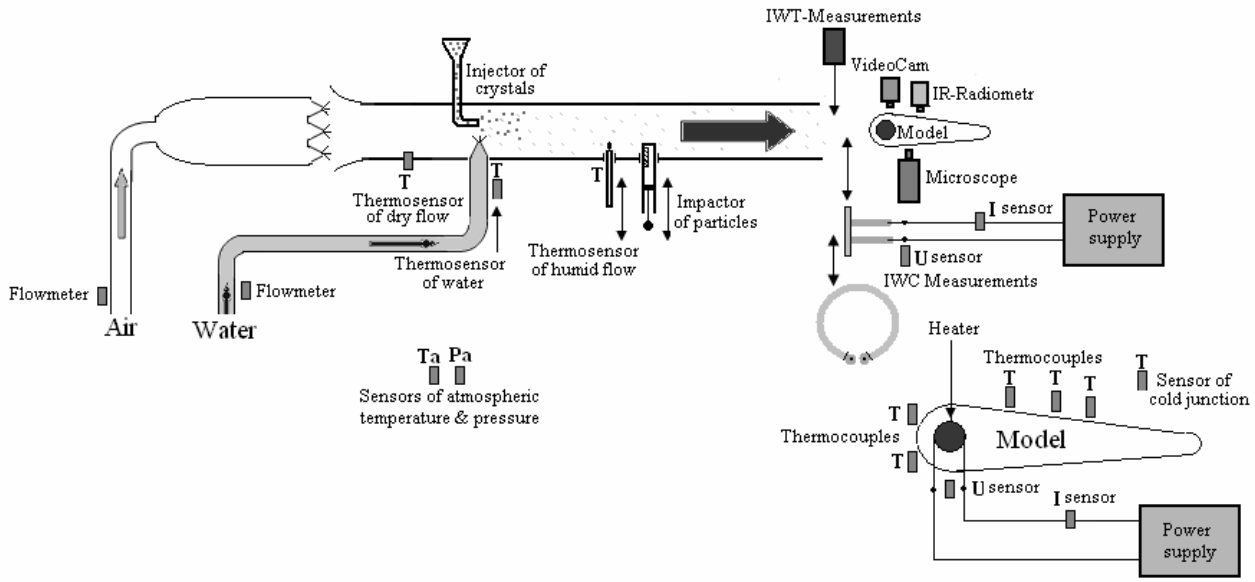

Figure 1: The schematic view of the EU-1 artificial ice facility and measurement resources

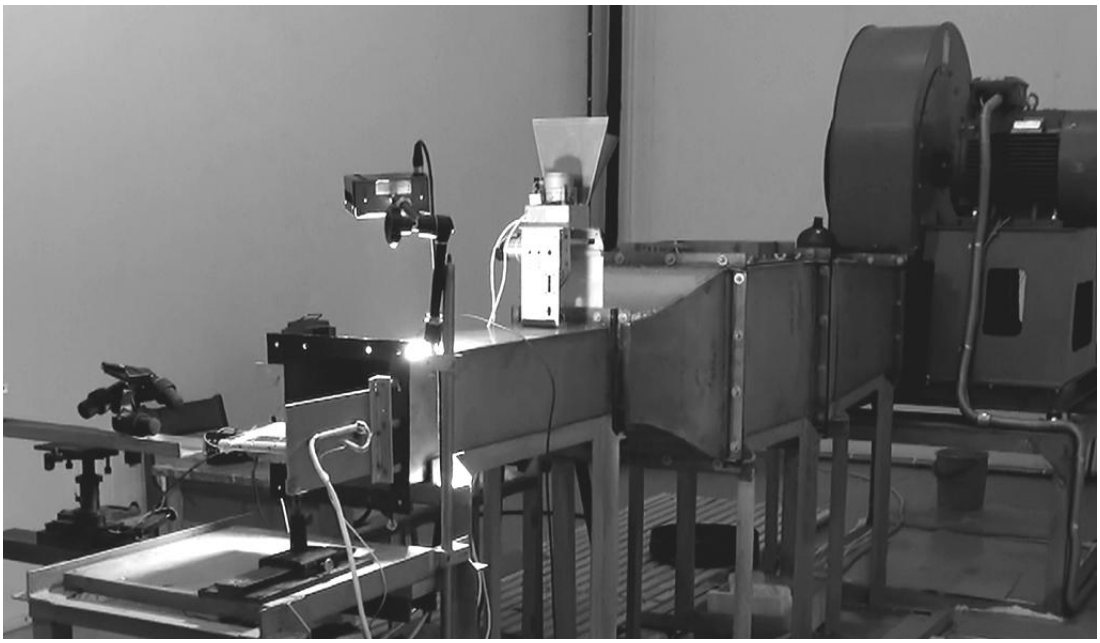

Figure 2: The year-round artificial icing rig

2.2 Test model

The test model is a wing airfoil with cylindrical front edge and flat surface areas on top and below. Figure 3 presents the model side view. The parts of the model are: 1 – front fairing, 2 – upper plate, 3 – upper backplane, 4 – lock bar, 5 – back fairing, 6 – back profile, 7 – lower backplane, 8 – supplement heating element, 9 – main heating element. All parts of the model are made from duraluminium D-16T. Circlets T1 – T8 show the places of thermocouples under model testing in “dry” air. Thermocouples for measurements in icing conditions were mounted in the body of leading edge and are not shown in figure.

DOI: 10.13009/EUCASS2017-314

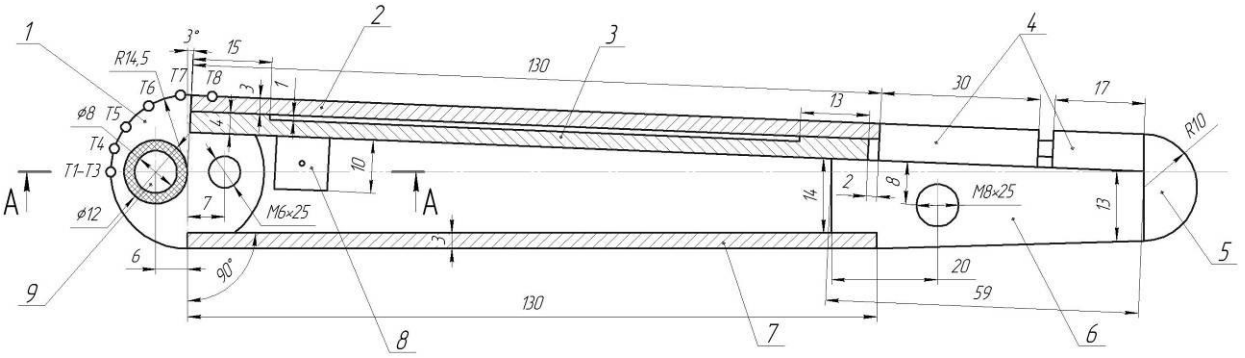

Figure 3: Test model, side view

2.3 Crystals characterization

Five main crystals types were used in experiments. Type 1 and type 2 are the crystals of newly fallen snow with MMD = 150 mkm and 430 mkm respectively, type 3 is the crystals with MMD = 1.3 mm produced in the blender from ice blocks by threefold working up. Type 4 is the crystals of type 3 were additionally machined in a grinder with rapidly rotating titanic knife. The processing kept on until the beginning of crystal agglomeration due to electrization. Then the crystals were supplied in the flow through the feeding unit with the rotating blades. The resulting MMD of type 4 is 180 mkm. Type 5 is the crystals of type 3 supported through rapidly rotating knifes to the air inlet of AWT fan and passed all the air dynamic channel length up to the working section. As a result the additional diminishing and separation of the crystals occurs, resulting crystals MMD = 530 mkm.

Crystals are catched in the AWT working section on the slide plate covered by the silicon oil or with aid of the L-shaped tube connected with the vessel. The second tube was provided to maintain the pressure in the vessel containing captured crystals equal to the static pressure of the flow. Crystals from plate or vessel were placed on the microscope slide and the photomicrographs were made. The computer analysis of the photomicrograph allows to find crystals area and their "size" – diameter of the circumcircle. The crystals third dimension was obtained from correlations [1] for natural crystals of type 1 and 2 or from direct measurement of their mean height for types 3, 4 and 5.

Figure 4 presents a typical view of the crystals of type 4 in the sample. Figure 5 gives diameter distribution of circumcircles resulted from processing a number of photos and the mass cumulative curve for MMD calculation.

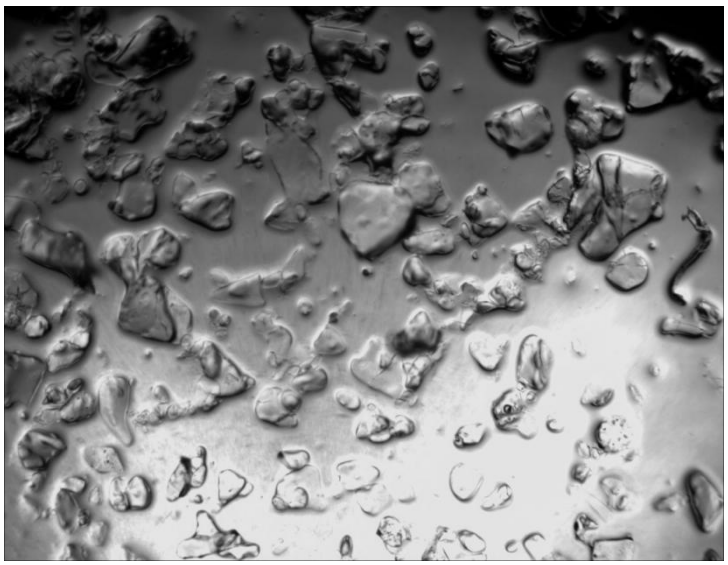

Figure 4: Crystals characteristic view, type 4. Figure total width is 2.5 mm

DOI: 10.13009/EUCASS2017-314

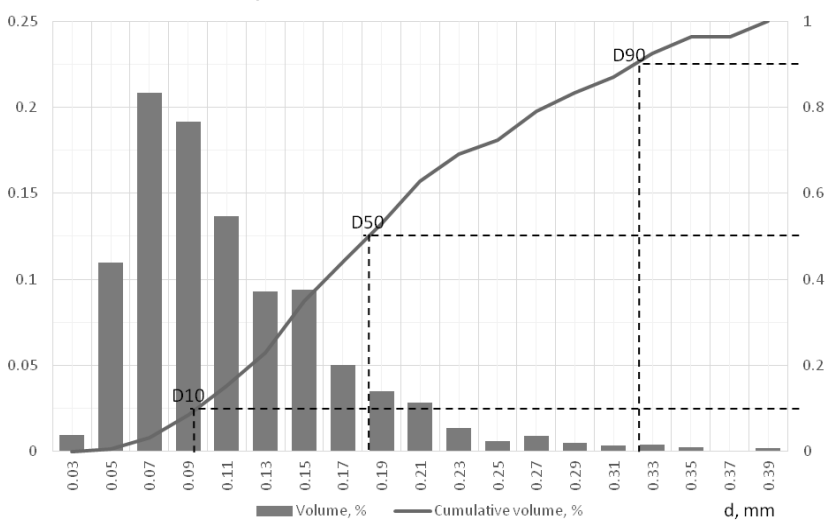

Figure 5: Crystals type 4 diameters distribution and the mass cumulative curve

2.4 Liquid film generation

The film on the model surface was generated with a swirl injector, placed upstream and below the model, as Figure 6 shows.

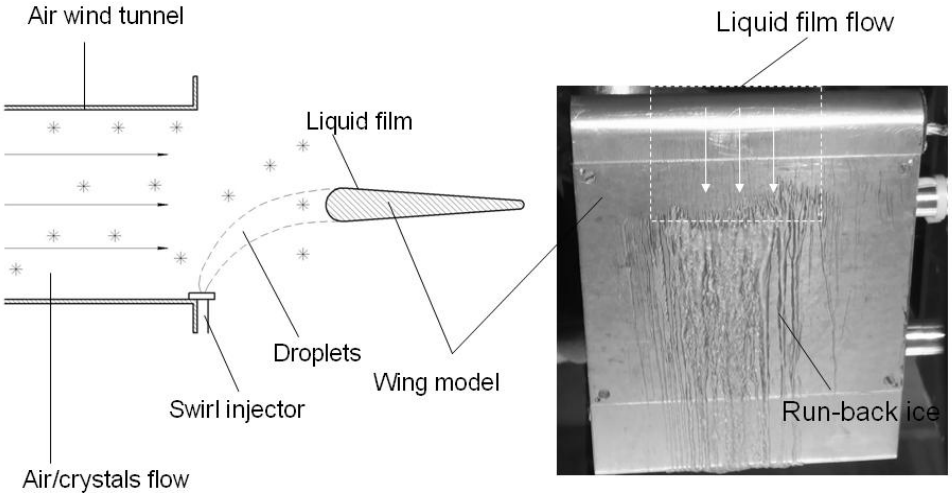

Figure 6: Generation of a liquid film on the model surface

The liquid flow thickness was measured by the system of high-speed micro video filming at aspect angle along the front edge of the wing. Figure 7*a* demonstrates a side view of a short portion of the model front edge before the beginning of liquid film generation, and Figure 7*b* presents the same portion with the flowing liquid film. The region of the film is observed as a light strip upside the model for the specially adjusted illumination. The film size is accessed by comparison with the size standard photographed at the same magnification. The film thickness lies in the range of 35–70 μm for all test conditions. Uncertainty of the thickness is due to non-stationary movement of the film along the surface.

DOI: 10.13009/EUCASS2017-314

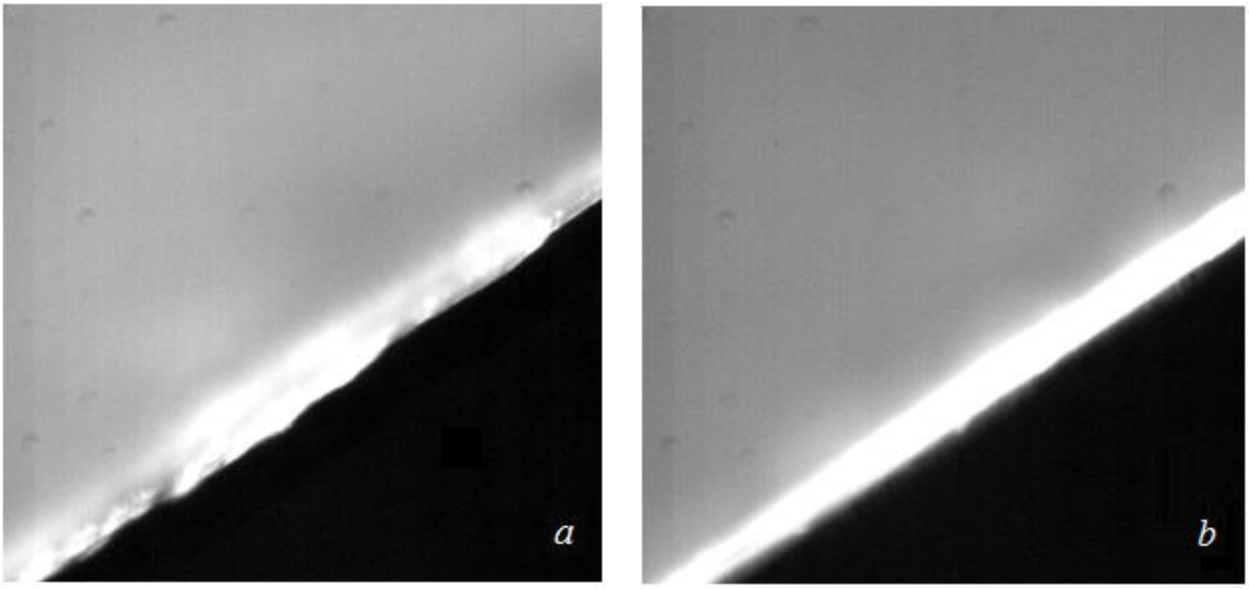

Figure 7: Portion of the model front edge (side view) before *a*) and after *b*) generation of the liquid film

2.5 Test procedure

Test procedure is as follows. The wing airfoil model was mounted in the tunnel as shown in Figure 1. Compressed air under pressure required for specified flow velocity was supplied in the wind tunnel. Voltage was applied to the heater, which warmed airfoil edge up to certain temperature in the range from 0 to 25^{o} C. On stabilizing the airflow parameters and model temperature field (thermocouple readings were observed by operator in real time mode) the crystals were supplied to the wind tunnel channel. From that moment the process of run-back ice formation was observed. In testing the process of run-back ice formation was video recorded and temperatures of airflow and model surface at the places of thermocouples were registered.

Experiment went on until the ice barrier formed, its height was less than 5 mm to ensure minimal water blow-off. After the barrier was formed, crystal supply was stopped. The model was cooled by airflow at slow velocity. After stop of the flow the upper plate with ice barrier was detached from the model, placed to the container to prevent from sublimation and weighed with precision balance. Thus we can ensure that the sublimation was negligible after flow stop. The sublimation mass loss was estimated from the videocamera observation. This effect can be significant for very small ice barriers and it becomes negligible for barriers with considerable height. In our tests sufficient ice height was provided for all experiments with liquid film and for the most part of the tests with dry surface. The arising uncertainty for small values of barriers masses was eliminated by the corrections on the basis of videocamera data and interpolation of test results.

In experiment one also determined IWC, total time of interaction of the model and ice-laden flow, position of the front border of run-back ice.

The similar procedure was during testing with liquid film generation. At first, without ice crystals in the flow the dependencies of generated run-back ice mass from water discharge and time interval of its injection on the wing front edge was obtained. Ice production was continued up to the thickness not greater than 5 mm. From this preliminary experiment one can access water losses due to its blowing off and evaporation. Then the experiment with supplying ice crystals in the flow was conducted. Mass of run-back ice was measured that allowing (with the preliminary experiment data taken into account) find the portion of crystals which stuck to the surface and accreted on it.

DOI: 10.13009/EUCASS2017-314

2.6 Thermodyamical processes in crystals cloud icing and methodology of experimental data processing

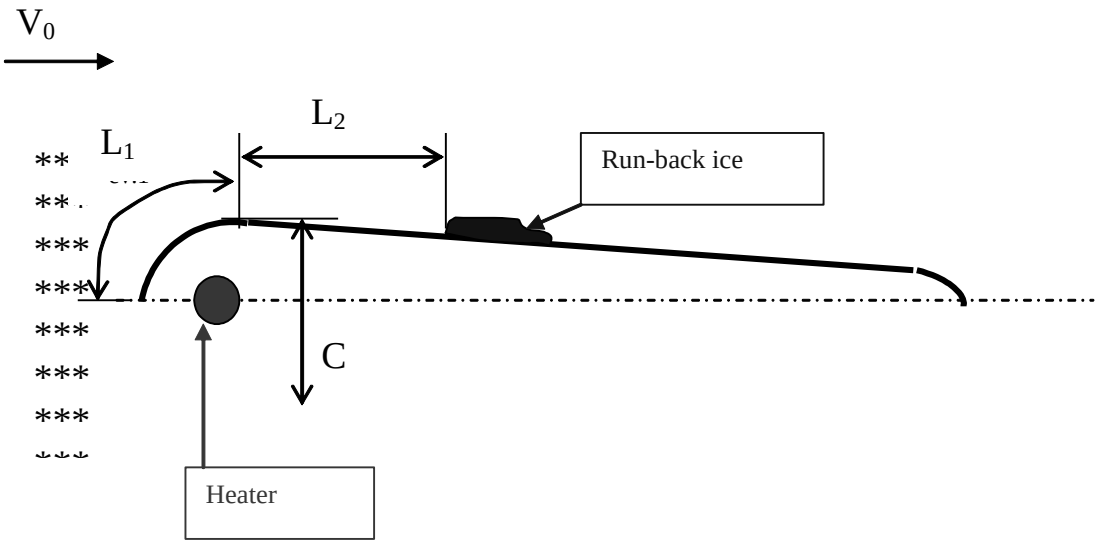

Figure 8: Geometrical interpretation of run-back ice formation on the upper side of airfoil

The following processes occur when crystals collide with the surface heated to positive temperatures. A portion of the crystals stick to the surface and melt completely. Some crystals melt partially, with their non-melt part being blown off the surface. Some crystal can be blown off (rebound) the surface immediately after the contact without melting. The melt portion of the crystals forms a water film, which partly evaporates and partly leaks to the surface area of negative temperatures to produce run-back ice (Figure 8). When water flows along the surface some amount of water is blown off. The blowing off effect is most apparent in forming run-back ice. Such physical model of the run-back ice formation can be considered as the improved Messinger model [2].

The crystal (partially melt or non-melt) blowing off process can be characterized by a certain coefficient of crystal blowing off (K_{BI}) equal to the ratio of the blown of crystal mass to the mass of crystals collided the surface. Besides, similar to water drops one can use the notion of total integral coefficient of collection, to be more precise it should be called the total integral coefficient of collision (E_B). A value of E_B equals the mass ratio of crystals collided with the surface to those which can collide.

Thus, the mass of crystals, which melt and formed a water film after colliding the surface (only the upper part) can be presented as follows

$$M_{RI} = E_B \cdot (1 - K_{BI}) \cdot V_0 \cdot \mathrm{IWC} \cdot C/2, \quad \mathrm{kg/(m\ s)}, \tag{1}$$

where IWC – ice water content, kg/m^3; V_0 – undisturbed flow velocity, m/s; $C/2$ – a half of airfoil midsection thickness (Figure 8), m. A value of M_{RI} is considered for a unit of time and running meter of airfoil.

The water film, as was mentioned, partially evaporates (M_{EW}), partially is blown off (M_{BW}), and partially forms run-back ice (M_{RBI}). If one neglects ice crystal sublimation then:

$$M_{RI} = M_{EW} + M_{BW} + M_{RBI} \tag{2}$$

Amount of evaporated water for the unit of time from a running meter of two airfoil parts (L_1 and L_2, Figure 1) can be obtained as

$$M_{EW} = M_{EW1} + M_{EW2}, \quad \mathrm{kg/(m\ s)}$$

For the part L_1:
$$M_{EW1} = 0.628\ \alpha_1 \xi_{s1} L_1 (e_{s1} - e_0)/(c_p p_0). \tag{3}$$

For the part L_2:
$$M_{EW2} = 0.628\ \alpha_2 \xi_{s2} L_2 (e_{s2} - e_0)/(c_p p_0), \tag{4}$$

DOI: 10.13009/EUCASS2017-314

where α_1, α_2 – mean heat transfer coefficients (W/(m^2 K)) for the surface area, where evaporation takes place; e_{s1}, e_{s2}, e_0 – saturated water vapour pressures (Pa) at temperatures T_{s1}, T_{s2} and T_0, respectively, (the air in the aerodynamic channel is very close to saturation in the case of the liquid film due to the droplets and film evaporation; in the case of the initially dry surface air is close to the saturation too due to the crystals sublimation and evaporation of film provided by melting crystals);
T_0 – temperature of the undisturbed flow, ^{o}C;
T_{s1}, T_{s2} – mean temperature of the wet surface on parts L_1 and L_2, ^{o}C;
p_o = 101325 Pa – air pressure at altitude H = 0 m;
c_p=1000 J/(kg K) – specific capacity of air;
L_1 – width of area along the chord, where crystals evaporate, m;
L_2 – width of area along the chord, where water film spreads or water drops move down to run-back ice formation zone, m;
ζ_1, ζ_2 –wetness coefficient, equaled to the ratio of wetted area to the whole area with inclusion of wetted.
Approximately one can suppose that $T_{s2} = (T_{s1} + 0)/2$ because the run-back ice formation starts on the surface part with temperature equal to 0 ^{o}C.
According to [3], one can assume $\zeta_1 = 1$ in the part L_1, and $\zeta_{,2} = 0.2–0.3$ in the part L_2.
The mass of run-back ice G_{RBI} formed on the airfoil is measured during the experiment. The run-back ice mass formed for the unit of time on one running meter of airfoil length is equal to:

$$M_{RBI} = G_{RBI}/ (\tau L_{su}) ,$$

where τ is the time of the run-back formation in s, L_{su} is the airfoil length in meters.
Amount of water, which is blown off by the airflow is not possible to estimate. So this amount should be considered together with the processes of crystal partially melting.

$$M_{BW} = K_{BW} E_B (1 – K_{BI}) V_0 C \text{ IWC}/2.$$

Here the coefficient of water blowing off (K_{BW}) is equalled to the ratio of amount of blowing off water to water formed due to crystal melting. From (1) and (2)

$$E_B (1 – K_{BI}) V_0 C \text{ IWC}/2 – M_{BW} = M_{EW} + M_{RBI}, \quad (5)$$

or

$$E_B (1– K_{BI}) (1– K_{BW}) V_0 C \text{ IWC}/2 = M_{EW} + M_{RBI} \quad (6)$$

The value $E_B (1– K_{BI}) (1– K_{BW})$ can be considered as the complex coefficient of water conservation, which reproduce the processes of partially ice collision with the surface and partially crystal and water blowing off the surface.

$$K_p = E_B (1– K_{BI}) (1– K_{BW}) = 2 (M_{EW} + M_{RBI})/ (V_0 C \text{ IWC}) \quad (7)$$

In experiments it is reasonable to find the dependency of K_p from IWC, V_0, T_s, T_0 and ice crystal MMD. The right hand side of Eq. (7) is estimated rather simple with some uncertainty.
For the surface part L_1 the mean heat transfer coefficient can be estimated by the expression for the cylinder streamlined in the perpendicular direction:

$$\text{Nu} = c \cdot \text{Re}^n = 0.023 \text{ Re}^{0.8}.$$

The cylinder diameter will be the characteristic dimension for the Re number. From the Nu number one can find the mean heat transfer coefficient

$$\alpha = \text{Nu} \cdot \lambda / L_1$$

For the surface part L_2 the mean heat transfer coefficient can be calculated by the expression:

$$\alpha = 0.0296 (\lambda / L) \text{Pr}^{0.33} \text{Re}^{0.8} ,$$

where λ is the air heat transfer coefficient; $L = L_1 + L_2$ is the distance from the airfoil stagnation point to the point of calculation; Pr – Prandtl number, which is equal to 0.71 for air; Re = VL/ν is the local Reynolds number; V – local flow velocity, ν – local cinematic viscosity coefficient for air.

DOI: 10.13009/EUCASS2017-314

Data processing was performed in the following way. The coefficient K_p values were estimated from (7) and its dependences from the difference of the temperatures T_{s1} and T_0, and also from the difference of the saturated water vapour pressures at these temperatures e_{s1} and e_0 were analyzed.
To describe the process in case of the liquid film presence all the above mentioned equations are valid, but the difference between total run-back ice mass due to water film and crystals ($M_{RBI\,2}$) and run-back ice mass due to water film only ($M_{RBI\,1}$) should be substituted for the value M_{RBI}. That is $M_{RBI} = M_{RBI\,2} - M_{RBI\,1}$. Besides, the values of $\zeta_1 = \zeta_2 = 1$ in the zones L_1 and L_2, since the solid water film is formed in the part L_1.

2.7 Test results in the case of crystals impingement on the dry warmed surface

The tests for the crystals impingement on the initially dry warmed surface were performed for three flow velocity values: 20, 45 and 80 m/s and for the flow temperature range –5.5 ...–18 °C, IWC range 3.3...18.1 g/m^3, mean temperature of the wet leading edge surface T_{s1} range –6...+21 °C. The test results are given for a number of runs in Table 1. Figure 9 shows example of the data processing results for the case with flow velocity 20 m/s in terms of K_p coefficient dependency from the temperature difference $\Delta T = T_{s1} - T_0$.
How one can see from the Table 1 and Figure 9 at a negative temperature of the flow slight heating of the model leading edge provides ice crystals adhering on the surface. Observations shown that a small part of crystals starts to adhere at the temperature of front surface $T_{s1} = -2.2$ °C ($\Delta T = T_{s1} - T_0 = 3.5$ °C). A process of adhering becomes stronger with rising of T_{s1}. At $T_{s1} = 0.6$ °C ($\Delta T = 6.3$ °C) on the front surface of the model appears a liquid film of water, which fully evaporates and flows away from the surface without leaking onto flat part of the model (no run-back ice).

Table 1: Test results in the case of initially dry surface

No	V_0, m/s	T_0, °C	IWC, g/m^3	T_{s1}, °C	P, W	Cryst. type	τ, s	G_{rbi}, g	L_2, mm	M_{imp}, g/(m s)	M_{rbi}, g/(m s)	M_{ew}, g/(m s)	K_p
2	20	-5.7	18.1	-2.1	11	1	120	0	0	5.249	0	0.002	0.0004
4	20	-5.7	18.1	0.6	28	1	120	0	0	5.249	0	0.004	0.0008
7	20	-8.8	8.3	3.3	88	2	180	0.7	0	2.393	0.026	0.009	0.0144
9	45	-8	3.3	9.3	141	2	375	0.23	50	2.153	0.004	0.037	0.0190
10	45	-8	12	6.8	132	3	45	0.39	40	7.83	0.058	0.028	0.011
14	45	-18	9.7	15	297	3	56	0.61	57	6.329	0.073	0.071	0.0228
22	80	-11.8	5	21.1	297	3	60	0	0	5.8	0	0.125	0.0216
24	80	-11.2	5	3.5	159	3	50	0	0	5.8	0	0.029	0.005
27	80	-9.4	10	6.1	212	3	128	0.49	16	11.6	0.026	0.039	0.0056

At T_{s1} =1.3 °C ($\Delta T = 10.4$ °C) thickness of liquid film greatly increases and a part of water starts to leak on the model's flat part allowing run back ice to grow up. Coefficient K_p increases from 0.0005 to 0.013 in the temperature range $T_{s1} = -2.2... - 1.7$ °C ($\Delta T = 3.5 - 10.8$ °C), which means portion of adhered and melted crystals becomes bigger. With further rising of temperature T_{s1} water film's thickness on the border between flat and cylinder part of model abruptly increases and the process of water blowing away enhances. It causes the reducing of runback ice's mass and, as a consequence, reducing of coefficient K_p. So, in the range of temperatures T_{s1} = 1.7 – 8.2 °C ($\Delta T = 10.8 - 16.3$ °C) the value of coefficient K_p reduces from 0.013 to 0.007.
Thus, on the rising temperature range we can pick out 4 temperature's areas with specific processes of crystals' adhesion, appearance and flow of the liquid film.
The first area – ice crystals adhere to the surface, but liquid film does not appear. The most quantity of crystals bounces away.
The second area – quantity of adhering crystals increases, liquid film forms, vaporizes and blows away in the adhering crystals zone.
The third area – quantity of adhering crystals still increases, liquid film leaks on the flat surface and runback ice appears. Mass of runback ice increases with increasing of surface temperature.
The fourth area – thickness of water film enlarges, volume of water blown away abruptly increases, runback ice's mass decreases, all processes stabilize on the area's boundary.

DOI: 10.13009/EUCASS2017-314

These four temperature's areas can have different borders depending on model's shape and two phase flow's parameters (air and ice crystals), but, probably, they still can be found for various combinations of model's shapes and flow's parameters.

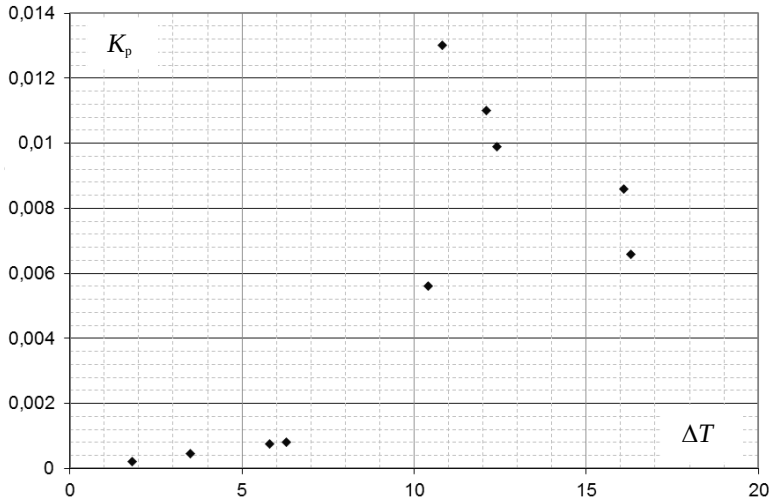

Figure 9: Dependency of K_p coefficient from the temperature difference $\Delta T = T_{s1} - T_0$

At flow velocity of 80 m/s and IWC of about 5 g/m^3 and in the range of wetted surface temperatures T_{s1} = 2.2 – 20.3 ^{o}C one can observe that the ice crystals stick to the front surface of the airfoil partially, and partially they melt down and evaporate. At that, the front surface temperature drops significantly. The amount of evaporated water at the front surface of the airfoil is in the range M_{EW1} = 0.024 – 0.12 g/(m s), that is of the same order as the water amount generated due to partial crystal fusion. As a result, the run-back ice on the flat part of airfoil does not form.

Table 2 presents a comparison of three runs. As one can see (run 1 and run 2), that at flow velocity of 20 m/s, IWC = 8.25 g/m^3 (natural snow), T_{s1} = 3.27 ^{o}C the amount of evaporated water M_{EW1} = 0.009 g/(m s). At that, the mass of run-back ice generated for the period of 180 s is 0.7 g at K_p = 0.011. Practically at the same temperature T_{s1} (+3,5 ^{o}C), but for the airflow velocity of 80 m/s, M_{EW1} = 0.03 g/(m s) (crushed ice, K_p = 0.005), and run-back ice did not form (M_{RBI} = 0).

This comparison shows that firstly the velocity increase from 20 m/s to 80 m/s results in the reduction of K_p almost doubly, i.e. the amount of crystals which stick to the surface, turn to water and keep on the surface as water film is reduced. Secondly, the amount of evaporated water at the front surface of the airfoil at V_o = 80 m/s increases almost 3.3 times and becomes greater than the mass rate of run-back ice generation of the case V_o = 20 m/s. Hence, water evaporation intensity in the region of crystal fusion signifies greatly for the generation of water film and for its flow.

Table 2 gives also run 3 data at the velocity of 80 m/s but IWC is greater doubly (10 g/m^3). At that, the run-back ice formed.

Table 2: Test results comparison at airflow speeds 20 m/s and 80 m/s

No	V_0, m/s	T_0, ^{o}C	IWC, g/m^3	T_{s1}, ^{o}C	τ, s	M_{RBI} g/(m s)	M_{EW1} g/(m s)	K_p
1	20	–8.8	8.25	3.27	180	0.019	0.009	0.011
2	80	–11.2	5	3.5	50	0	0.03	0.005
3	80	–9.4	10	6.1	128	0.49	0.039	0.005

DOI: 10.13009/EUCASS2017-314

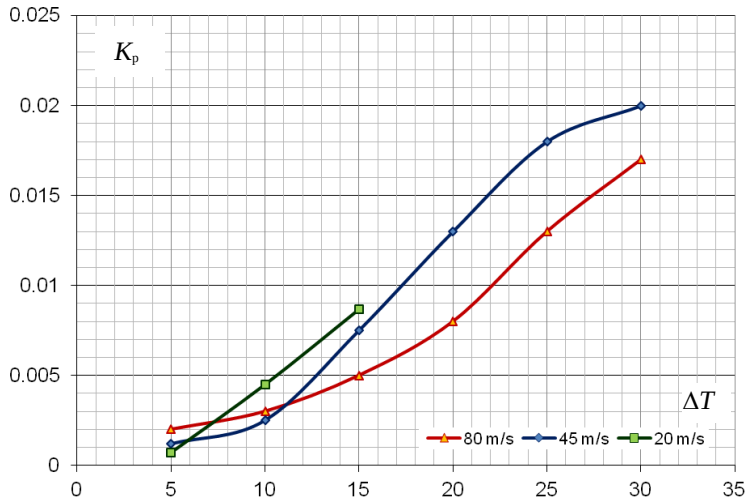

Figure 10: Dependency of K_p coefficient from the temperature difference $\Delta T = T_{s1} - T_0$ at different speeds of airflow

Figure 10 presents the influence of airflow velocity. In the range ΔT = 12 – 30°C the coefficient K_p tends to an decrease when airflow velocity increases from 20 to 80 m/s since crystal blowing off the surface is apparently reduced. At ΔT = 5 – 11 °C this trend is broken due to evident disorder (irregularity) of crystal sticking and blowing off the surface.

2.8 Test results in the case of crystals impingement on the heated surface with liquid film

Tests results at velocities 20 m/s, 45 m/s and 80 m/s are presented in Table 3. When flow velocity is 20 m/s and crystals are present, the amount of runback ice is increasing in comparison with the case when liquid film flows without crystals (runs 35-36, table 3). Experiments with wide range of IWC variation showed that when crystals' content in the flow increases, the mass of the runback ice decreases. Increasing of liquid water content as well as flow velocity leads to the growth of crystals' flow towards the liquid film, which gives the effect of the runback ice mass diminution.
At flow velocity 45 m/s when crystals are added to the flow the amount of runback ice mass may be more or less than in regimes with liquid film only.

Table 3: Experimental results and K_p values for the case of airfoil heated surface with liquid film

No	V_0, m/s	T_0, °C	IWC, g/m^3	T_{s1}, °C	P, W	Cryst. type	τ, s	G_{rbi}, g	L_2, mm	M_{imp}, g/(m s)	M_{rbi}, g/(m s)	M_{ew}, g/(m s)	K_p
35	20	-13.3	0	6	119	-	60	3.31	8.7		0.368	0.013	
36	20	-13.4	10	0	119	3	60	6.44	15.1	1.450	0.716	0.011	0.248
6	45	-15	0	18.7	271	-	61	4.32	66		0.472	0.079	
8	45	-15	15	11.4	292	3	65	7.95	43	4.894	0.815	0.046	0.080
16	45	-14	4.2	13.9	292	4	70	8.45	45	1.370	0.805	0.054	0.282
18	45	-14	4.7	15.8	292	4*	60	0.51	51	1.533	0.057	0.063	0.078
23	80	-10.9	0	1.4	119	-	60	5.5	16		0.611	0.025	
26	80	-10.8	11	-1.2	119	3	60	0.82	0	6.380	0.091	0.015	-0.079

* : in this run liquid film was not created, run-back ice was produced only by crystals

At the air velocity 80 m/s the total mass of the runback ice diminished when crystals were added to the flow in all investigated cases. The characteristic view of the run-back ice on the model surface is shown in Figure 11*a* (run 23, liquid film only) and in figure 11*b* (run 26, liquid film and impinged crystals). The mass of the run-back ice formed during 60 s of experiment was decreased more than 6 times when crystals were added to the flow, table 3. Crystals' diminution from MMD = 1.3 mm to 0.18 mm leads to a small increase of K_p, however runback ice mass becomes smaller than when liquid film flows without crystals with the same supplied heater power.

DOI: 10.13009/EUCASS2017-314

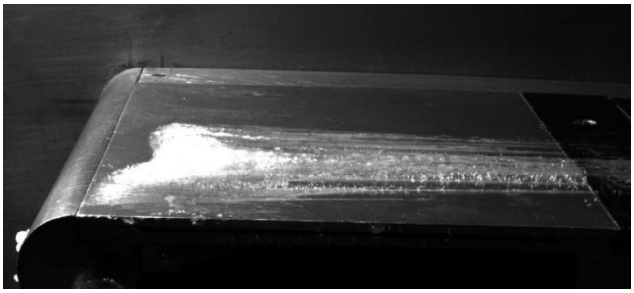

Figure 11*a*: Characteristic view of the run-back ice for the run 23 of Table 3, liquid film only

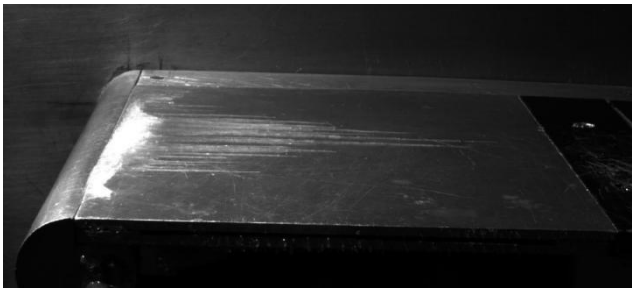

Figure 11*b*: The same for run 26 of Table 3, the run-back ice was formed by liquid film and impinged crystals

The comparison of K_p in cases of ice crystals impingement to liquid film at flow velocities 20, 45 and 80 m/s is presented in Figure 12. K_p values can become negative due to some current ratios between values of vaporized water mass (M_{EW}) and amount of runback ice formed from ice crystals only (M_{RBI}= $M_{RBI\ 2}$ – $M_{RBI\ 1}$). i.e. sign of value (M_{EW} + M_{RBI}) designates K_p sign.

So, when the impinging crystal mass M_{imp} is not large enough, liquid film captures crystals effectively. In this case the mass of run-back ice is greater than in the cases of runback-ice provided by the liquid film or crystals separately. At the same time one can observe a tendency of diminution of K_p when flow velocity increasing in the case of dry surface as well as in the case with presence of liquid film. In the initially dry surface case the most probable reason of this phenomenon are effects of crystals and liquid film blowing off which increase with the flow velocity growth. In the case of liquid film this effect also can be caused by the cooling of the model which is due to crystals as a well as their destructive effect on a liquid film (stimulation of waves, splashing, taking over of water when crystal rebounds from surface).

Thus, test results provided the conclusion that interaction of large amount of crystals with the surface is completely differs from the corresponding single crystal interaction.

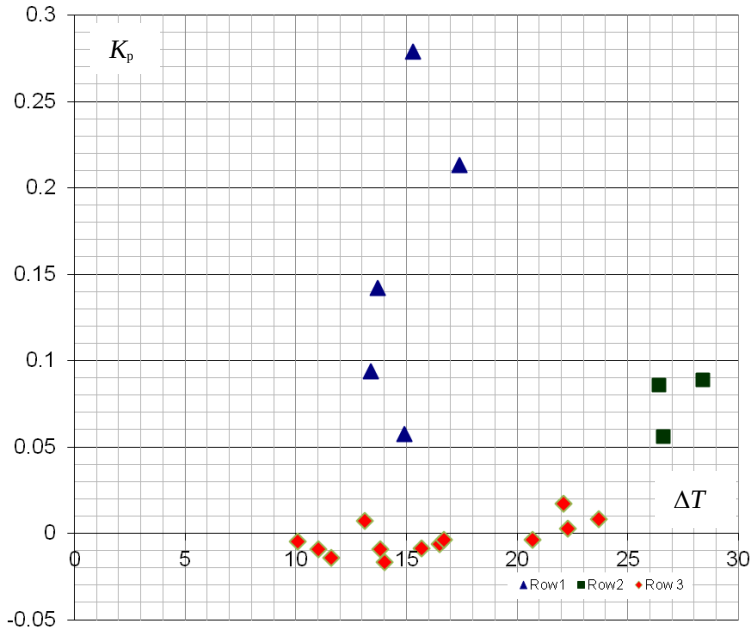

Figure 12: Dependency of K_p coefficient from the temperature difference $\Delta T = T_{s1} - T_0$ in regimes with ice crystals and liquid film added at different speeds of airflow: Row 1 – V_0 = 20 m/s, Row 2 – V_0= 45 m/s, Row 3 – V_0 = 80 m/s

3. Theoretical investigations

Theoretical investigations concerned the modeling of the water film streaming along the surface of a body, which is inserted in airflow with ice crystals. The mathematical model for the hydro-thermodynamic behavior of the film, carrying the penetrated crystals, was developed. The model takes into account the dependence of the effective viscosity of the suspension on the mass fraction of the dispersed phase in the solidifying film and the finite time of

DOI: 10.13009/EUCASS2017-314

crystal melting. The developed model was tested for the description of water film flow along the surface of a circular cylinder for the case of film generation due to water infusion through a horizontal slot at the front critical line of the cylinder. Such a method of film generation was used in the earlier TsAGI experiments. The detailed results of this part of investigations were published in [4].
The main technique of film generation on the body in TsAGI experiments was water injection by sprayer near the front part of the model. The developed mathematical model [4] can be easily modified for this case (in the absence of crystals in airflow).
The boundary layer equations averaged with respect to the film thickness h_l were used for the description of film hydro-thermodynamics. The system of equations includes the equations of film continuity, momentum and energy as follows

$$\partial \rho_l h_l \langle u_l \rangle / \partial x = -\rho_i \partial h_i(x,t)/\partial t - \dot{m}_{\text{phas}} + \dot{m}_{\text{imp}}, \tag{8}$$

$$0 = -h_l\, dp/dx + \tau_+ - \tau_w + \dot{m}_{\text{imp}} u_p, \tag{9}$$

$$\partial \rho_l h_l \langle u_l T_l \rangle / \partial x = \dot{q}_+ - \dot{q}_w - \dot{m}_{\text{phas}} L_v + \dot{m}_{\text{imp}} \left(V_p^2/2 + c_l (T_p - T_f) \right). \tag{10}$$

Here ρ_l is liquid film density, $\langle u_l \rangle$ is mean velocity of the film flow, x is coordinate along the surface, ρ_i is ice density, h_i is thickness of ice layer, formed due to solidifying of the film; $\dot{m}_{\text{phas}}$ is flux density of water mass output from the film due to evaporation; $\dot{m}_{\text{imp}}$ is flux density of mass input to the film by incoming liquid particles; p is film pressure, which is determined by the external flow; τ_+ and τ_w are friction stresses at the outer and inner (wall) film boundaries. The last term in Eq. (9) allows for the momentum of incoming particles (u_p is their velocity along the film). Then T_l is film temperature, $\dot{q}_+$ $\dot{q}_w$ are heat flux densities at the outer and inner film boundaries, L_v is latent heat of water/vapour transition, V_p is absolute value of liquid particle velocity under collision with the film, c_l is specific heat capacity of water, T_f is temperature of water freezing/ice fusion (273 K).
A part of water, flowing along the surface, may turn into ice, therefore a sink appears in Eq. (8) in the first term of the right-hand side. One can find the ice thickness growth rate from the balance of the heat released during phase transformation and the one which is removed from the ice layer due to:

$$\frac{\partial h_i(x,t)}{\partial t} = -\frac{\alpha_l (T_l^+ - T_f)}{\rho_i L_s}, \tag{11}$$

where α_l is coefficient of heat transfer from ice to the film, T_l^+ is temperature of the film outer boundary, L_s is latent heat of ice/water transition.
We specified the velocity $u_l(y)$ and temperature profile $T_l(y)$ (y is coordinate perpendicular to the surface) of fluid motion in the film by the expressions

$$u_l(y) = y(1 - 0.5y/h_l)\tau_w/\mu_l + 0.5y^2\tau_+/(h_l\mu_l),$$
$$T_l(y) = T_w + y(1 - 0.5y/h_l)dT_l/dy\big|_w + 0.5(y^2/h_l)dT_l/dy\big|_+.$$

These presentations allow obtaining average values $\langle u_l \rangle$ and $\langle u_l T_l \rangle$ in Eqs. (8) and (10).
Energy flux densities $\dot{q}_+$, $\dot{q}_w$ were taken in the form

$$\dot{q}_+ = \alpha_a (T_\infty - T_l^+),\ \dot{q}_w = \alpha_l (T_l^+ - T_w),$$

where α_a is heat transfer coefficient from the film surface to airflow, T_w is wall temperature.
As earlier [4], we used the expression for α_a from [5], obtained from computation of cylinder local heat transfer in the region of no separation of laminar flow. The cylinder surface is assumed to be adiabatic, i.e. $\alpha_l = 0$, in the region $x < x_f$, where x_f is coordinate, at which T_w drops below T_f. Further heat transfer coefficient α_l is not equalled to zero yet. It is assessed on the base of the computed value of $\langle u_l T_l \rangle$ under the condition of $T_w = T_f$. The obtained value of α_l would allow assessing the icing rate $\partial h_i/\partial t$, given by Eq. (11). Pressure p in the film was obtained in the assumption of a potential flow around a “dry” cylinder. The well-known expression for shear stress τ_+ in the form of Blasius series corresponds to the pressure distribution.

DOI: 10.13009/EUCASS2017-314

The initial condition for the film velocity was $u_{l0} = 0$ at $x = 0$. In carrying out computations, we adjusted the value of the drop mass concentration ρ_p in the main flow, for the water flow rate at the top of the cylinder ($\theta = \pi/2$) to be equalled to 1 g/s (the value is given out by experimenters). Besides, the value of drop temperature is adjusted, for the initial wall temperature T_w to be equalled to 276 K.

Calculations were done for three values of incident airflow velocity u_∞ = 20, 50 and 80 m/s. Figure 13 demonstrates numerical results for the film thickness. In contrary to the case of film pressing out through the slot, the film thickness is enhanced steadily. But the film is much thinner that one can expect for generation of water/crystal suspension. The calculated film thickness in the latter case is in good agreement with the measurements, which gave film thicknesses in the range 35–70 mkm.

Figure 14 presents distributions of the film flow velocity. The results of velocity calculations for both methods of film production coincide qualitatively, but the velocity of film motion for the latter case is lower.

Figure 15 gives the distribution of film temperature. One can see that the film does not reach the temperature of freezing at the front part of the cylinder.

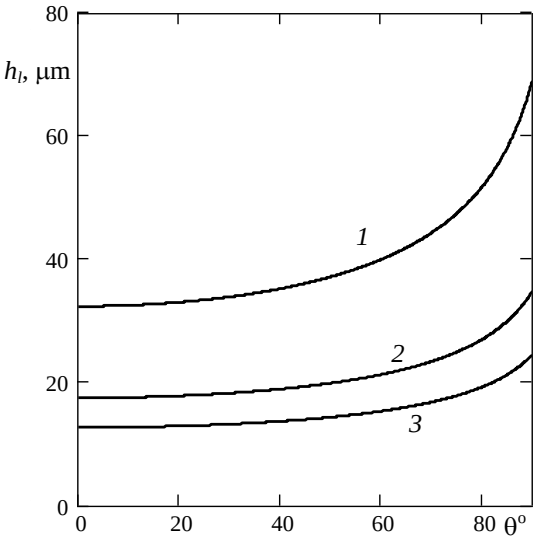

Figure 13: Variation of the film thickness along the cylinder contour at the different velocities of incident airflow:
1 – 20, *2* – 50, *3* – 80 m/s

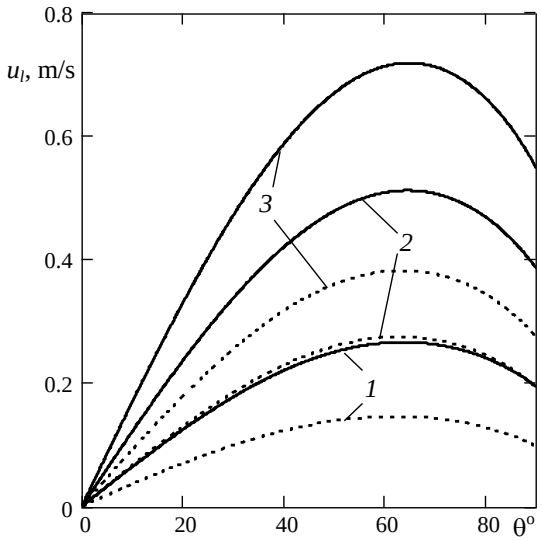

Figure 14: Variation of the film velocity along the cylinder contour.
Solid lines – u_l^+, dashed ones – $\langle u_l \rangle$.
Specification as in Figure 13

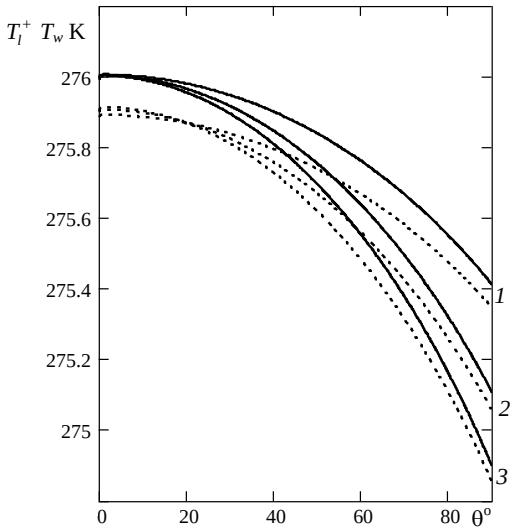

Figure 15: Dependencies of the film temperature.
Solid lines – temperature of lower boundary (wall) T_w, dashed ones – upper boundary T_l^+.
Specification as in Figure 13

DOI: 10.13009/EUCASS2017-314

Now we are working on computation of the film flow along the whole surface of the test model (wing airfoil with cylindrical front edge and flat surface areas, Figure 3).
Firstly, we have computed the flow of ideal liquid around the test model. An approximate method of conformal mapping, namely, the method of trigonometric interpolation [6], has been used for this. Figure 16 presents the distributions along coordinate x of laminar boundary layer outer flow velocity $U(x)$ and corresponding value of $-dp/dx = UdU/dx$. The latter enters Eq. (9). The distributions of $\tau_w(x)$ and $\alpha_a(x)$ are required to implement our mathematical film model. They have been obtained by numerical integration of the well-known boundary layer equations [7]. Figure 17, 18 present distributions of these parameters (ρ_a, λ_a are air density and heat conductivity, R is radius of the front cylindrical part of the model, $\mathrm{Re} = u_\infty R/\nu_a$ is Reynolds number). The obtained results will allow computing film hydro-thermodynamics.

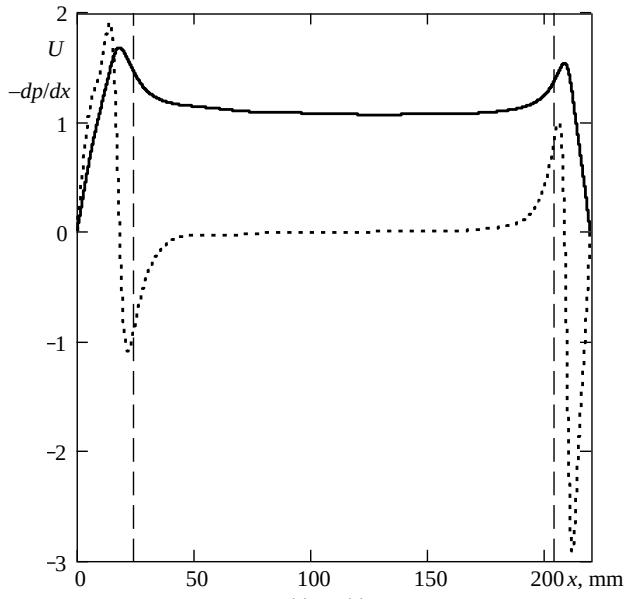

Figure 16: Distributions of the outer velocity (solid line) and pressure gradient (dashed one) in the film along the coordinate x of the model surface. Vertical lines mark the boundaries of the flat part of the model

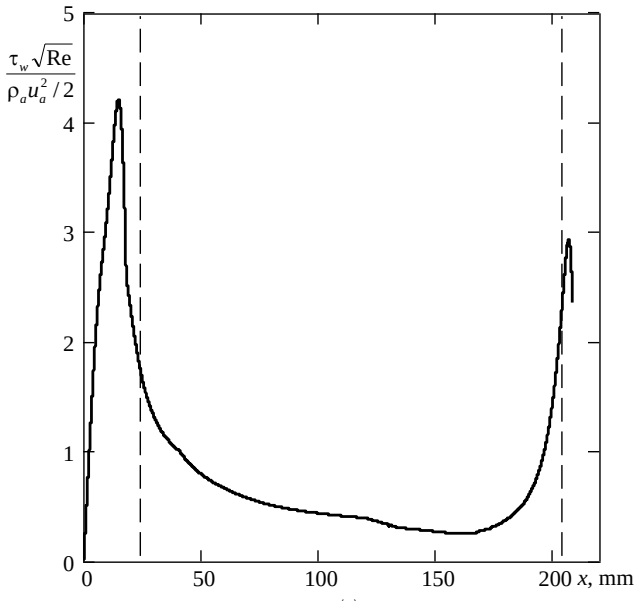

Figure 17: Distribution of the shear stress

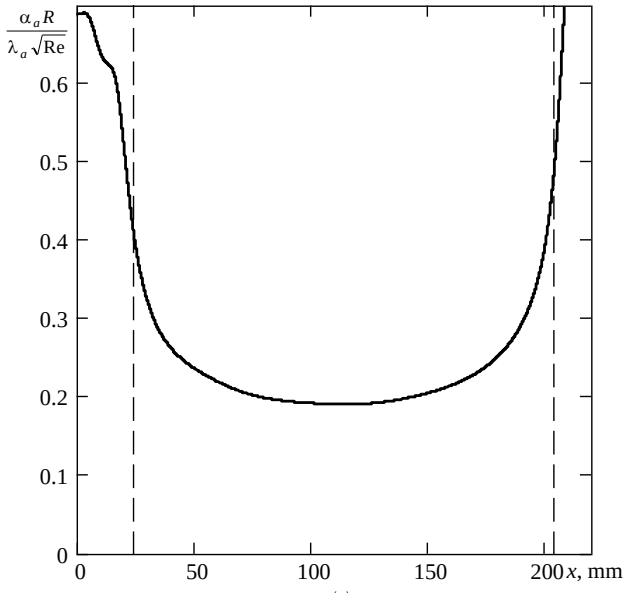

Figure 18: Distribution of heat transfer coefficient

DOI: 10.13009/EUCASS2017-314

Conclusions

1 On the base of investigations of moving ice crystals interaction with heated surface, the integrated coefficient K_p of water generation and conservation on the surface was developed. The coefficient reproduces the processes of partial collisions of crystals with surface, partial crystals fusion in their partial blowing-off (bounding-off), partial crystallization of spreading water under partial blowing off the surface.
2 Analysis of dependency of coefficient K_p from difference of temperature of wet surface T_{s1} and temperature of undisturbed flow T_0 shows that value of K_p at experimental conditions varied in the range from 0.004 to 0.02 for the case of initially dry surface. This testifies that only 0.4 – 2% of mass of the crystals impinged the surface converts to water, which takes part in evaporation and formation of run-back ice. The rest of crystal mass is blown off the surface either before fusion or after fusion during water film flow along the surface.
3 With generating the additional water film (thickness 35-70 μm) on the front surface of airfoil, the value of K_p increases approximately up to 3 – 4.5 times at crystal MMD of 1.3 mm. At crystal MMD of 0.18 mm , the value of K_p increases greater (almost 7 fold). This testifies that the additional water film assist to keeping ice crystals on the airfoil surface, finer crystals being kept stronger. The maximal values of K_p up to 0.28 were obtained at flow velocity 20 m/s.
7 Coefficient K_p diminishes when air flow velocity increases. It can be explained as follows - additional liquid film, in one hand, better keeps crystals on surface, in another hand, probably destroyed by the flow of crystals. At flow velocity 80 m/s K_p value decreases rapidly and can even become negative.
8 Tendency of K_p decreasing with increasing of flow velocity was observed in both types of experiment – with dry surface and with liquid film on it. In both cases blow off effects, strengthening with higher velocity cause this tendency. This engages us to consider the interaction of large amount of crystals with surface as individual phenomenon, which includes additional physical mechanics unlike the interaction of single crystal with surface.
9 The way forward can include the detail investigation of the crystals and water blowing off and the study of the crystals-to-surface interaction in the case of liquid film presence.
10 On the base of the developed physico-mathematical model the calculations were carried out of the evolution of the film thickness, velocity and temperature along the leading edge of the experimental model in the cross air/crystal flow. The calculated film thickness is in good agreement with the measurements. The obtained results for distributions of pressure gradient, shear stress and heat transfer coefficient make it possible to compute the film flow along the whole surface of the test model.

Aknowledgments. The part 2 of this work was performed in the frames of the European Union 7th Framework Programme Project HAIC – High Altitude Ice Crystals under grant agreement nACP2-GA-2012-314314 and the part 3 was supported by the Russian Science Foundation under grant 16-19-10472.

References

[1] Heymsfield A. 2003. Properties of tropical and midlatitude ice cloud particle ensembles. Part I: Median mass diameters and terminal velocities. *Journal of the Atmospheric Sciences.* Vol. 60. 2573 – 2591.
[2] Messinger R.L. 1953. Equilibrium temperature of an unheated icing surface as a function of air speed. *Journal of the Aeronautical Sciences.* Vol. 20. No. 1.
[3] Tenishev R. Kh., Stroganov B.A. et al. 1967. Aircraft anti-icing systems. Moscow: Mashinostroenie (in Russian).
[4] Kashevarov, A.V., Stasenko, A.L. 2017. Hydro-thermodynamics of a liquid film with crystals on the body surface in an air flow containing ice particles. *J. Appl. Mech. Techn. Phys.* Vol. 58. No. 2. 275–284.
[5] Zukauskas, A.A. 1982. Convective heat transfer in heat exchangers. Moscow: Nauka (in Russian).
[6] Fil'chakov, P.P. 1964. Approximate methods of conforming mapping. Kiev: Naukova Dumka (in Russian).
[7] Schlichting, H. 1955. Boundary-layer theory. NY: McGraw-Hill.